ELSEVIER

Marine Geology 225 (2006) 157–175

MARINE GEOLOGY
INTERNATIONAL JOURNAL OF MARINE GEOLOGY, GEOCHEMISTRY AND GEOPHYSICS

www.elsevier.com/locate/margeo

Mineralogy and geochemistry of hydrothermal sediments from the serpentinite-hosted Saldanha hydrothermal field (36°34′N; 33°26′W) at MAR

Ágata S. Dias *, Fernando J.A.S. Barriga [1]

CREMINER, Department of Geology, University of Lisbon, Edificio C6, Piso4, Campo Grande, 1749-016 Lisboa, Portugal

Received 14 March 2005; received in revised form 24 July 2005; accepted 26 July 2005

Abstract

The Saldanha hydrothermal field is located at the top of a serpentinized massif (Mount Saldanha, MS) at a non-transform offset (NTO5) along the Mid-Atlantic Ridge (MAR), south of the Azores. It is one of the rare known sites on a worldwide basis where direct evidence of low-temperature (7–9 °C) hydrothermal activity has been provided by direct observation of hydrothermal fluid venting through small orifices in the ocean floor sedimentary cover. This study focuses on the mineralogy and geochemistry of 14 sediment cores collected at MS. For comparison, four samples collected at the Rainbow site (NTO6) were also studied. Mount Saldanha hydrothermal sediments are highly "diluted" within a dominant foraminiferal nanofossiliferous ooze with small fragments of underlying rocks. The mineral assemblage of the hydrothermal component is characterized by sulphides, nontronite, smectites, poorly crystallized Mn oxyhydroxides and amorphous material. Cu, Zn and Fe sulphides, Mn–Mg oxy-hydroxides and putative manganobrucite were also identified in one sample collected at an orifice vent. In this sample, micro-chimneys (conduits) composed of isocubanite and sphalerite were also identified. Mount Saldanha sediments show a clear enrichment in elements such as Mn, Mg, Fe, Cu, P and V, derived from hydrothermal fluids, and Ni, Cr and Co, derived from ultramafic rocks. The geochemical data together with the observed mineral assemblage suggest that the hydrothermal fluids are at a higher temperature than those measured at the escape orifices (7–9 °C), and a strong enrichment in Mg, mainly at the top of the mount, agrees with extensive mixing of the hydrothermal fluid with unmodified seawater. Nevertheless, the mineral assemblage of MS sediments is consistent with the precipitation from hydrothermal fluids at much lower temperatures than at Rainbow. The presence of serpentinized and steatitized (talcshist) ultramafic rocks and the occurrence of a strong methane anomaly within the overlying water column collectively suggest that the hydrothermal circulation at MS is driven by exothermic reactions closely associated with the serpentinization process. Rainbow sediments have a higher concentration in transition metals and consequently an enrichment in sulphides. These differences are likely to be a consequence of the higher temperature of hydrothermal fluids, reflected in the composition of hydrothermal solutions, and of a stronger hydrothermal flux at the Rainbow site.

Keywords: Hydrothermal sediments; Mount Saldanha hydrothermal field; low-temperature vents

1. Introduction

The Saldanha hydrothermal field is located at the Mid-Atlantic Ridge (MAR), south of Portugal's Azores

* Corresponding author. Tel.: +351 21 750 0000x26463; fax: +351 21 759 9380.
E-mail addresses: Agata.Dias@fc.ul.pt (Á.S. Dias), F.Barriga@fc.ul.pt (F.J.A.S. Barriga).
[1] Tel.: +351 21 750 0000; fax: +351 21 759 9380.

0025-3227/$ - see front matter © 2005 Elsevier B.V. All rights reserved.
doi:10.1016/j.margeo.2005.07.013

Archipelago (36°34′N; 33°26′W), between the Pico Fracture Zone (PFZ), 38°N, and the Oceanographer Fracture Zone (OFZ), 35°40′N (Fig. 1A). This region of the MAR is composed of six left-lateral non-transform offsets (NTOs) (Detrick et al., 1995; Gràcia et al., 2000). These offsets are characterised by peridotite massifs detached from their segment flanks and are frequently associated with hydrothermal vents (Fouquet et al., 1997; German et al., 1996). The exposure of ultramafic rocks is consistent with low magma budgets, relatively thin crust and irregular faulting patterns (Gràcia et al., 2000). Mount Saldanha (MS) is located on NTO5, between the FAMOUS and AMAR second-order segments (Fig. 1B), and consists of a faulted massif detached from its segment flanks, almost parallel to the ridge segment. It is composed mainly of ultramafic and gabbroic rocks.

In this area, Charlou et al. (1997) and Bougault et al. (1998) reported important methane anomalies with low TDM (total dissolved manganese) levels, detected during the FLAME (Charlou et al., 1997; German et al., 1997), HEAT (German et al., 1994, 1996) and FAZAR (Koeppenkastrop and De Carlo, 1992; Langmuir et al., 1992; Charlou et al., 1993) cruises, raising the expectation of the presence of a hydrothermal field. This was investigated with dives during the FLORES cruise (Fouquet et al., 1998) without success. However, serpentinites and other ultramafic rocks were recovered suggesting hydrothermal activity related to serpentinization. Confirming these predictions, the MS

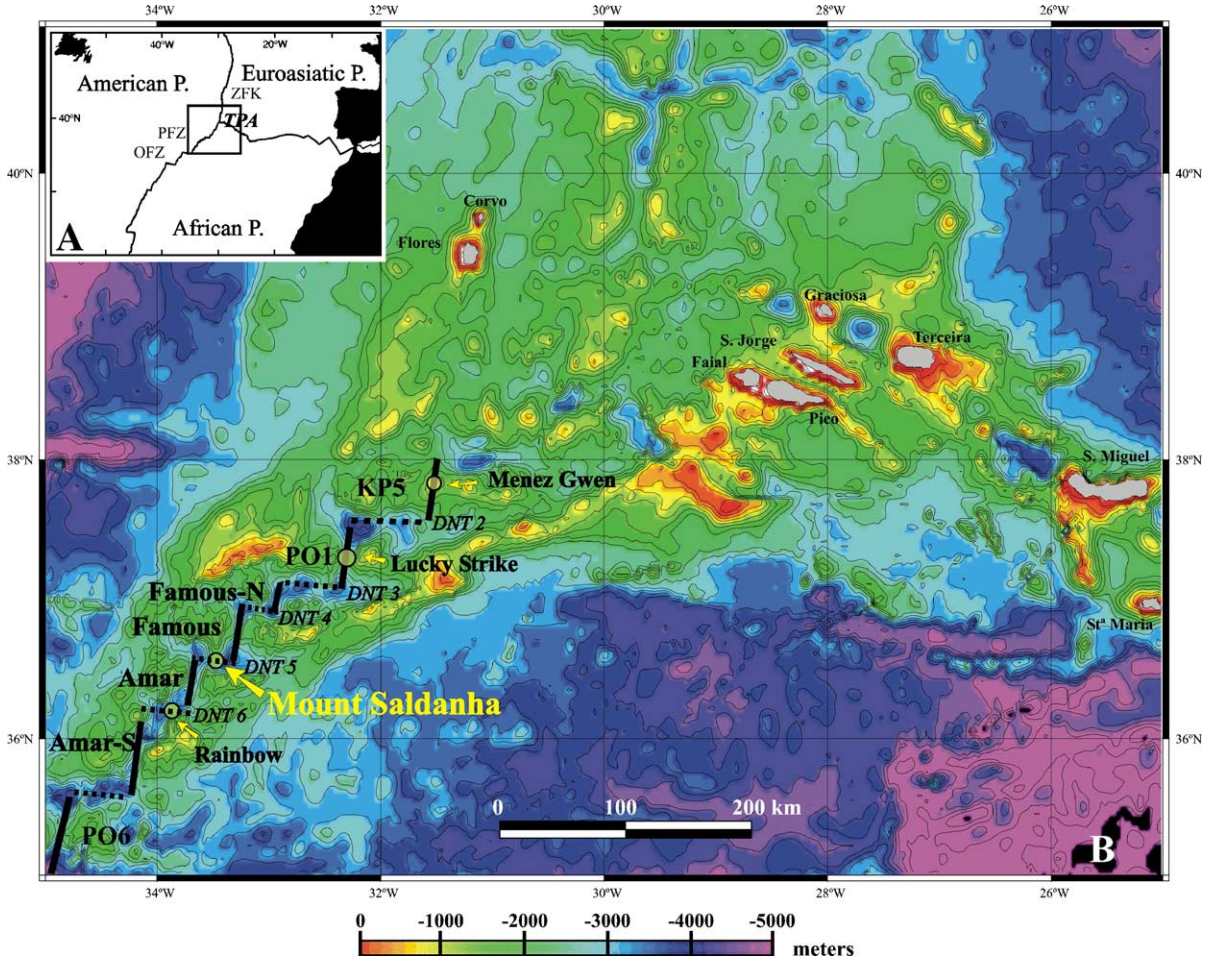

Fig. 1. (A) Area between the Pico Fracture Zone (PFZ) and the Oceanographer Fracture Zone (OFZ) along the Mid-Atlantic Ridge, south of Azores Triple Junction (TPA); (B) relief map showing the location of Mount Saldanha at a non-transform offset (NTO5) between FAMOUS-S and AMAR segments, and Rainbow at a non-transform offset below Mount Saldanha (NTO6), between AMAR and AMAR-S segments. These two sites are hosted on peridotite and serpentinized peridotite massifs. The relief map was prepared by J. Luis, N. Lourenço and M. Miranda and the non-transform offsets (dashed lines) and individual spreading axes (black lines) are projected according to Gràcia et al. (2000) and Parson et al. (2000), respectively.

hydrothermal field was discovered in 1998 during the SALDANHA cruise (Barriga et al., 1998). At the summit of a seamount (MS), hydrothermal fluid venting through centimetric orifices in the ocean floor sedimentary cover was directly observed over an area of approximately 400 m^2 and at depths between 2200 and 2220 m. Rock samples classified as peridotites, serpentinites and steatites (also known as talcschists and soapstones) were recovered, which, together with field observations, made it possible to map the area (Costa, 2001). In situ temperature measurements of the discharge fluid at the hydrothermal orifices revealed fluid temperatures of 7–9 °C, whereas the adjacent seawater next to the seafloor was at around 2 °C (Barriga and Seahma Teem, 2003).

The source of the heat at the MS hydrothermal field has been suggested to be derived from the exothermic serpentinization process (Barriga et al., 1998). There are only three other hydrothermal fields, all at MAR, where hydrothermal fluids derived from ultramafic reactions have been described: the Rainbow (Fouquet et al., 1998; German et al., 1996) and the Logatchev (Bogdanov et al., 1997), with high-temperature fluids; and the Lost City (Kelley et al., 2001), with low-temperature fluids.

However, the source of heat in these ultramafic-hosted hydrothermal systems is controversial. Although heat production in these systems has often been directly linked to the exothermic nature of the olivine to serpentinite reaction (Fyfe, 1974; Barriga et al., 1998; Kelley et al., 2001; Bach et al., 2002; Lowell and Rona, 2002; Schroeder et al., 2002), several authors argue that these reactions do not produce enough heat to explain peridotite-hosted hydrothermal systems (e.g., Allen and Seyfried, 2004). For example, an additional heat source has been suggested for the Logatchev and Rainbow sites (Allen and Seyfried, 2003; Lowell and Rona, 2002). Heat balance models by Lowell and Rona (2002) suggest that heat released upon serpentinization of peridotites can explain hydrothermal venting only at temperatures ranging from a few degrees to a few tens of degrees Celsius, as happens at MS (7–9 °C, Barriga and Seahma Teem, 2003). Bach et al. (2002) reached the same conclusion after calculating that the serpentinization process can heat up circulating water to 25–150 °C. Thus, although higher temperature ultramafic hydrothermal systems, such as the Rainbow, seem to depend on an additional magmatic heat source, it seems possible that low-temperature systems, such as MS, are exclusively driven by the serpentinization exothermic process. Additional data on the geochemistry, mineralogy and geophysics of these systems are needed to clarify this issue.

Diffuse flow at hydrothermal systems seems to constitute the major flux of heat and chemical transfer at the seafloor. Hydrothermal sediments can conceivably hold distinct hydrothermal components: (1) near-field components derived from corrosion and mass-wasting of seafloor hydrothermal deposits; (2) distal plume-related components (Mills and Elderfield, 1993); and (3) components directly precipitated from hydrothermal fluids that percolate through the sediments (German et al., 1995; Mills et al., 1996).

Unlike many other systems sampled so far along the MAR, at MS, the hydrothermal discharge takes place through the sediments, which seem to form an impermeable cover, blanking the system. Thus, the hydrothermal fluids react not only with the underlying crystalline rocks but also with the sedimentary cover. The hydrothermal component of the sediments precipitates from percolating fluids. This could also take place at the more sedimented parts of the Rainbow field. Here, the hydrothermal component is largely dominated by more or less corroded sulphides resulting from fall-out and mass wasting of seafloor hydrothermal deposits. These deposits completely cover up a possible hydrothermal component resulting from within-sediment precipitation.

In order to identify the hydrothermal component of MS sediments, their mineralogical and geochemical properties are described. The data are compared with hydrothermal sediments collected at Rainbow and occasionally with previously published geochemical data from other MAR hydrothermal sediments. Because the MS hydrothermal system has the lowest venting temperature so far described, the study of its sediments could prove particularly valuable in order to understand the nature of ultramafic-hosted systems that putatively lack a magmatic heat source.

2. Sampling and analytical methods

Sampling was carried out in July 1998 with Ifremer's manned submersible *Nautile*. Eight dives were performed and a 40-cm 'push-corer' was used to recover 14 short (27 cm maximum) cores of hydrothermal sediments at MS, one of which (SF13) was sampled in a small hydrothermal vent orifice (Fig. 2 and Table 1). For comparison, four samples were also collected at Rainbow during the same cruise. Three of those sediments were sampled near black smoker chimneys and a fourth sample (SR2) was collected at a zone of diffuse discharge (Table 1).

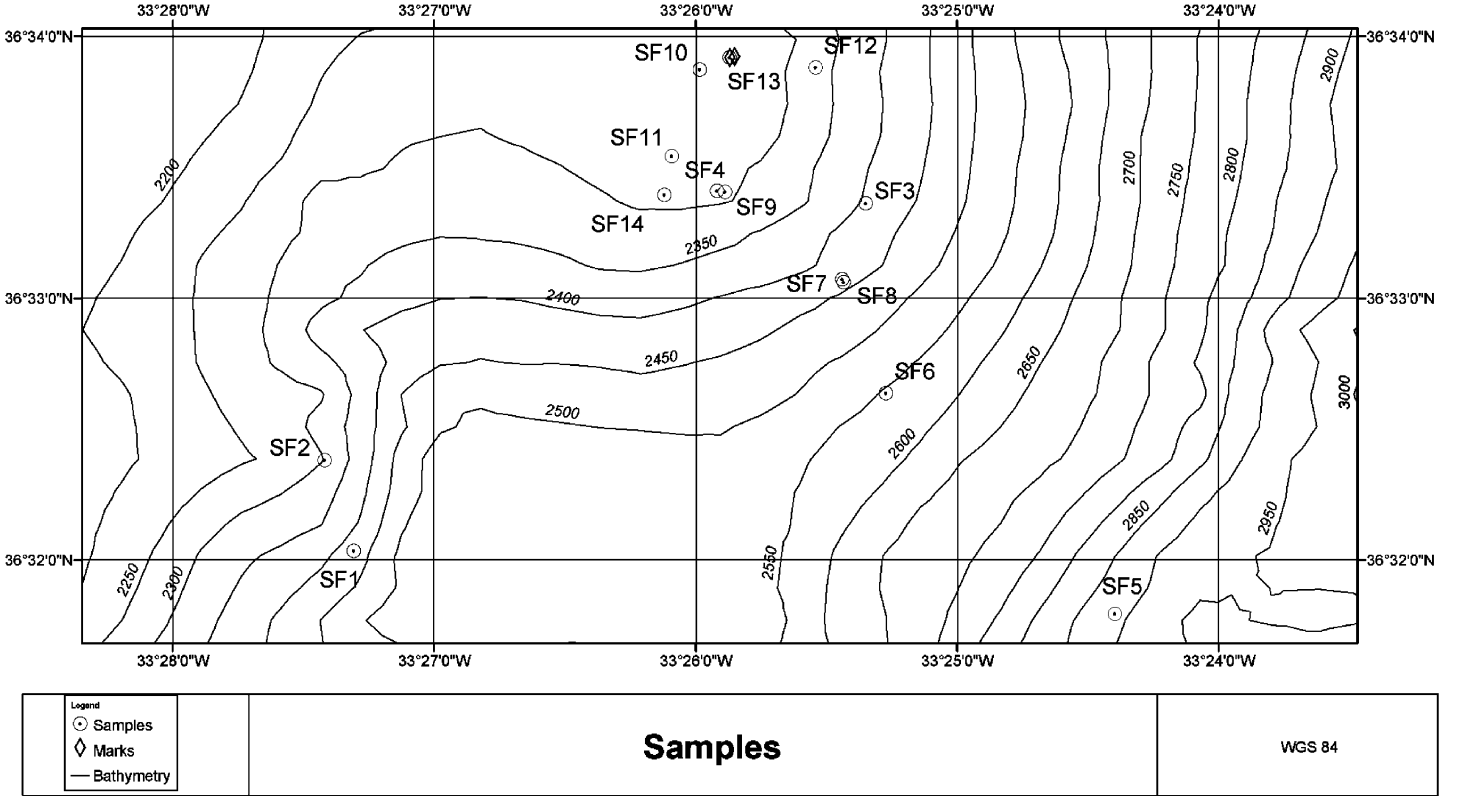

Fig. 2. Map of Mount Saldanha with location of the 'push-corers' (circles) and respective sample number. The square represents the hydrothermal area where centimetric holes exhaling a white hydrothermal fluid at 7–9 °C have been identified. SF13 sample was collected exactly at one of these holes.

Table 1
General macroscopic description of Mount Saldanha and Rainbow 'push-corers'

Samples	Length sediment recovered (cm)	General description	Rock fragments	Other relevant information	Distance to the venting orifice (m)
Mt Saldanha					
SF1	16.5	Pale brown carbonate ooze	Fresh basalts	Collected at a deep fault	4095
SF2	22.0	Pale brown carbonate ooze	Fresh basalts		3672
SF3	20.0	Pale brown carbonate ooze	Gabbros		1286
SF4	14.0	Pale brown carbonate ooze	Fresh basalts		954
SF5	27.5	Pale brown carbonate ooze	Serpentinites	Collected near a scarp	4513
SF6	11.0	Pale brown carbonate ooze	Serpentinites and a few altered basalts	Collected near a scarp	2544
SF7	(a)	Whitish pale brown carbonate ooze	Serpentinites	Collected near a scarp	1726
SF8	(a)	Whitish pale brown carbonate ooze	Serpentinites	Collected near a scarp	1681
SF9	(b)	Whitish pale brown carbonate ooze	n.i.		944
SF10	17.0	Pale brown carbonate ooze	Steatites		190
SF11	24.0	Pale brown carbonate ooze	Steatites and some fresh basalts		771
SF12	(b)	Whitish pale brown carbonate ooze	Steatites and some fresh basalts		503
SF13	13.5	Greyish pale brown carbonate ooze with some whitish veins	Steatites	Collected exactly at a hydrothermal vent	0
SF14	19.0	Pale brown carbonate ooze	n.i.		1035
Rainbow					
SR1		Reddish material with some massive sulphides and pelagic carbonates	Steatites	Collected near black smoker chimneys	
SR2		Reddish pale brown carbonate ooze	Some steatites and few steatites	Collected in a very sedimented zone with diffuse discharge	
SR3		Reddish material massive sulphides	Some steatites	Collected near black smoker chimneys	
SR5		Reddish material massive sulphides and pelagic carbonates	Serpentinites	Collected near black smoker chimneys	

(a): Semi-consolidated sediment; (b): consolidated sediment; n.i.–not identified because of the small size of the rock fragments.

The majority of MS sediment corers collected are pale brown carbonate oozes, except the more consolidated samples, which are whitish. Frequently, the sediments contain fragments of underlying rocks such as gabbros, serpentinites, steatites (talcshists) and basalts (up to 7 cm long). The three Rainbow sediments collected near the black smokers are reddish dark brown, rich in sulphides and correspondingly poorer in carbonates. The SR2 Rainbow sample was similar to MS sediment but somewhat darker.

Samples collected at MS were analysed for their mineralogy and geochemical composition of bulk sediments. Prior to any type of analyses, all samples were dried at less than 25 °C. Optical microscopic observations of the sediments were performed on polished thin sections. In order to achieve an effective polish, the sediment samples were consolidated by impregnation with an epoxy resin.

X-ray diffraction (XRD) of the sediments' $<4\Phi$ fractions and of some selected manganese oxides particles was performed using a Philips PW 1710 diffractometer with CuKα radiation generated at 40 kV and 49 mA. The material was analysed on a pure silicon sample holder (PW 1817/32) because it does not produce interferences and requires less material for analysis than other sample holders. The $<4\Phi$ fraction was examined after air drying and glycol saturation treatments. Data were interpreted using Creminer's in-house "XRD-Identify" software, developed by Carlos Carvalho (in preparation).

As the sediments have a very high carbonate content, leaching with a 10% HCl solution of sample aliquots was necessary to study the mineralogy of the insoluble residual grains. As other minerals besides carbonates could have been leached by this process, the major elements in the resultant acid solution were quantified by atomic absorption analyses. Polished thin sections of the insoluble residue were made as described above and optical microscopic observations were conducted. Chemical analyses

were conducted on representative polished thin sections of the insoluble residue using a three-channel wavelength dispersive JEOL SUPER PROBE 733 electron microprobe, operated at an accelerating voltage of 18 kV and at a beam current intensity of 25 nA. Natural minerals and pure metal standards were used before, during and after each analytical session. The precision of the measurements was better than 2% for the major elements.

To complement the mineralogical characterization, geochemical analyses were carried out on the bulk sediment. Determination of major and minor elements and rare-earth elements (REE) concentrations were made by Inductively Coupled Plasma Optical Emission Spectrometry (ICP), Inductively Coupled Plasma Mass Spectrometry (ICP-MS) and Instrumental Neutron Activation Analysis (INAA). Carbon and S concentrations were determined by LECO (see Appendix for further details). All geochemical analyses were carried out at "Activation Laboratories, Ltd" (ACTLABS, Ontario, Canada) following standard procedures. The standards used by Actlabs were SY3, MRG1, W2, DNC1, BIR2, G2, NBS, STM, IF-G and AC-E and specifically for REE were MAG1, BIR1, DNC1, GXR2, LKSD3, MICA-Fe, GXR1, SY3, STM and IFG1. The measurement precision for the major oxides was better than ± 1–2%, and for the other elements, the precision was generally better than 5–10%. Specifically, for REE, the measurement precision was 5% or better.

To determine the hydrothermal component of major elements in MS bulk sediments, data from BOFS (Biogeochemical Ocean Flux Study) cores were used to define background elemental levels (data from Cave et al., 2002). Those cores are appropriate to be used as a background since they are pelagic sediments without hydrothermal influence and were collected in similar latitudes at the MAR and in similar depositional environments.

Rare-earth elements (REE) data were normalised to the REE concentrations of chondrites (Taylor and McLennan, 1985). The deviation of Ce and Eu from the rest of REE can be expressed as Ce anomaly (Ce/Ce*) and Eu anomaly (Eu/Eu*) where * refers to the value obtained by linear interpolation between adjacent elements.

3. Results

Microscopic characterization of bulk sediment revealed that MS samples are mainly calcareous oozes made up of biogenic calcite (foraminiferal and coccolith tests) with hydrothermal precipitates and small fragments of lithoclasts and minerals from the underlying rocks.

Mount Saldanha sample aliquots treated with HCl were almost totally soluble, revealing their high carbonate content. Samples collected at Rainbow had a lower content of soluble material (Table 2).

The more consolidated samples (SF7, SF8, SF9 and SF12) had a higher content of soluble material, while three of the sediments collected near hydrothermal orifices (SF13, SF10 and SF11) and also sample SF1 presented a lower content of soluble material (Table 2). Insoluble residues were formed by hydrothermal components and detrital lithoclasts. The observed differences between MS and Rainbow samples suggest different proportions of the carbonate and hydrothermal fractions.

The presence of major elements in the solution resultant from the acid attack was investigated with atomic absorption analyses in order to understand if HCl digested other minerals besides carbonates. The proportion of each major element relative to the total of analysed elements in MS samples is represented in Fig. 3. Calcium is the main element present, representing more than 60% of the total of dissolved major elements. A lower Ca concentration (about

Table 2
Average and standard deviation (wt.%) of the material digested with HCl in aliquots from each sample

	Average	S.D.
Mount Saldanha		
SF1	84.78	4.83
SF2	94.81	2.79
SF3	94.33	0.85
SF4	95.59	0.21
SF5	94.99	1.56
SF6	95.31	0.42
SF7[a]	98.25	0.50
SF8[a]	95.69	1.18
SF9[a]	96.06	0.58
SF10	86.81	4.24
SF11	90.03	2.98
SF12[a]	97.86	0.64
SF13	91.47	6.50
SF14	95.17	0.19
Average	93.65	1.96
Rainbow		
SR1	54.10	5.36
SR2	85.70	–
SR3	28.00	5.73
SR5	71.10	–
Average	59.73	5.55

[a] Consolidated or semi-consolidated sediments.

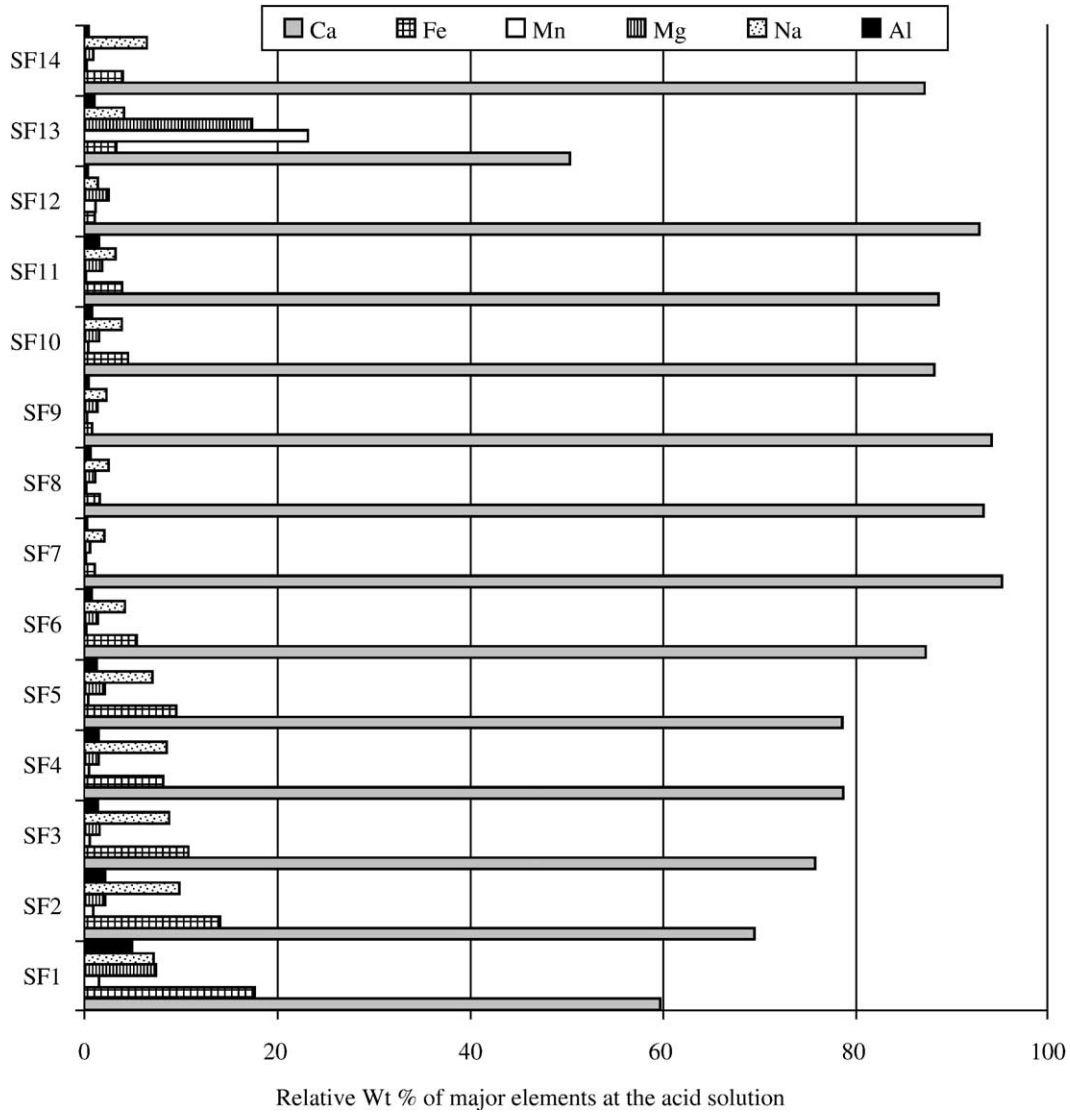

Fig. 3. Relative percentage of the major soluble elements in the acid solution resultant from the HCl attack to the MS sediments determined by atomic absorption analysis.

50%) was observed in sample SF13, collected at an active hydrothermal orifice. In this sample, the combined Mn and Mg content amount to about 40% of the total. Thus, although the dissolved major elements do not exclusively represent the carbonate fraction, the HCl leaching procedure provides, with a few exceptions, a reasonable estimate of the carbonate content.

The presence of Fe, Mn and Mg in the solution probably derived from poorly crystalline oxides and hydroxides. Some Fe could also have originated from sulphides dissolved with the acid solution. Sodium and Al in samples with small amounts of Fe, Mg and Ca were probably derived from clay minerals.

3.1. Mineralogy

The mineralogy of MS sediments determined by XRD and optical and electron microprobe analyses revealed, besides carbonates, the presence of serpentine, talc, olivine, plagioclases, clay minerals and Mg, Fe and Mn minerals. The sediment content in olivine, pyroxenes, serpentine and talc correlate with the abundance of different lithoclastic grains and, consequently, with the different lithologies of the underlying rocks. For example, talc was mainly identified from steatite grains present in sediments collected at the top of MS where this lithology was more abundant. Fine-grained pyrite and sometimes

isocubanite were observed disseminated in all sediments. Sphalerite and putative manganobrucite were also observed in sample SF13. Sulphide minerals were rarely observed and were normally anhedral grains smaller than 0.1 mm in diameter. In most samples, it was not possible to obtain accurate quantitative electron microprobe analyses due to polishing problems and/or to the small size of the sulphide grains. Sediment SF13 exhibits a larger quantity of sulphides, including larger grains. Reflected light microscopy revealed the presence of pyrite, isocubanite and sphalerite.

Isocubanite and pyrite occur in isolated grains and exhibit a deficient polishing. Pyrite also occurs as local replacement in foraminiferal tests, and isocubanite occasionally occurs in association with sphalerite, the former surrounding the latter (Fig. 4A). Averages of closely similar electron microprobe analyses on these minerals revealed the following chemical compositions:

Isocubanite (Icb): $(Cu_{0.97},Co_{0.03},Ni_{0.01})_{0.97}Fe_2S_3$;
Pyrite (Py): $(Fe_{0.937},Co_{0.002},Cu_{0.002})_{0.941}S_2$
Sphalerite (Sph): $(Zn_{0.72},Fe_{0.18},Cu_{0.001},Co_{0.01})_{0.91}Fe_1S_2$

At the top of the SF13 core, it was possible to observe millimetric tubular structures formed by Icb and Sph. These have been interpreted to be micro-chimneys (Fig. 4B and C) similar to those described by Usui et al. (1997). The outer walls of these structures were formed by cemented sediment and oxyhydroxides aggregates. At the inner wall, sulphide and oxide minerals were observed, as well as a non-identified pale green mineral. Some radiolarian tests were also observed inside the tubes. This morphology and mineral zonation are consistent with previous descriptions of micro-chimneys (Haymon and Kastner, 1981; Haymon, 1983; Zierenberg et al., 1984; Fouquet et al., 1993; Hannington et al., 1995; Lafitte et al., 1985).

In Rainbow sediments, fragments of Icb and Sph with a similar microscopic concentric zonation were also observed (Fig. 4D). These were present in larger quantities and were better polished than in MS sediments. The mean chemical analyses for Icb and Sph in Rainbow sediments showed the following composition:

Icb: $(Cu_{0.97},Co_{0.05})_{1.02}Fe_{2.05}S_3$ and
Sph: $(Zn_{0.66},Fe_{0.29})_{0.94}Fe_1S_2$

The formation of Sph with a higher percentage of Fe at Rainbow is consistent with what has been described for reduced and warmer hydrothermal fluids (Deer et al., 1982; Ames et al., 1993; Hannington et al., 1995).

All samples contain amorphous material at the $<4\Phi$ fraction in the insoluble residue, as shown by XRD (Fig. 5). Only one diffractogram of this fraction is shown because all analyses were similar. They depict a broad elevation centred near 25° 2θ. This feature corresponds perfectly to the amorphous silica pattern.

X-ray diffraction also revealed the presence of smectite–clorite and nontronite. Nontronite (Al-poor Fe-smectite) is particularly abundant in three of the samples collected near the hydrothermal orifices (SF10, SF11 and SF13). The presence of nontronite has been reported in various other seafloor hydrothermal deposits (e.g., Bischof, 1972; Bonatti et al., 1972; Hoffert et al., 1978; Alt, 1988; Hékinian et al., 1993; Severmann et al., 2004). Experimental data on nontronite synthesis (Harder, 1976) suggest that the solution from which this mineral forms has a low temperature (3 to 29 °C), nearly neutral pH (7–9) and is slightly reduced ($E_h = -0.2$ to -0.8). However, oxygen isotope thermometry from TAG metalliferous sediments shows that nontronite formation may occur at up to 90 °C (Severmann et al., 2004). Aoki et al. (1996) also mentioned that the mechanism of formation of Fe-rich clay minerals is attributed to the interaction of Si, Al and Mg from the seawater with a Fe-rich hydrothermal solution flowing through the sea floor. At MS, the presence of sulphide minerals suggest that nontronite could have formed at higher temperatures than those of the hydrothermal fluids (7–9 °C, Barriga and Seahma Teem, 2003). The lower temperatures measured at the orifices are probably a consequence of cooling effects during conductive circulation and seawater interactions.

Poorly crystalline Mn-oxides minerals occur mainly in the sediment collected at the venting orifice (SF13). They usually form collomorphic bands and concretions that comprise intimate mixtures of more crystalline and less crystalline manganese oxides, identified by XRD as todorokite and vernadite/birnesite, respectively. High reflectance bands comprise the more crystalline specimens and low reflectance bands comprise the poorly crystalline ones, which are also not as well polished (Fig. 4E–H).

The mean of poorly crystalline Mn-oxides microprobe analyses are shown in Table 3. The totals were lower than 90%, and as microprobe qualitative analyses did not detect elements other than those listed, the remaining percentage was considered to be H_2O^+.

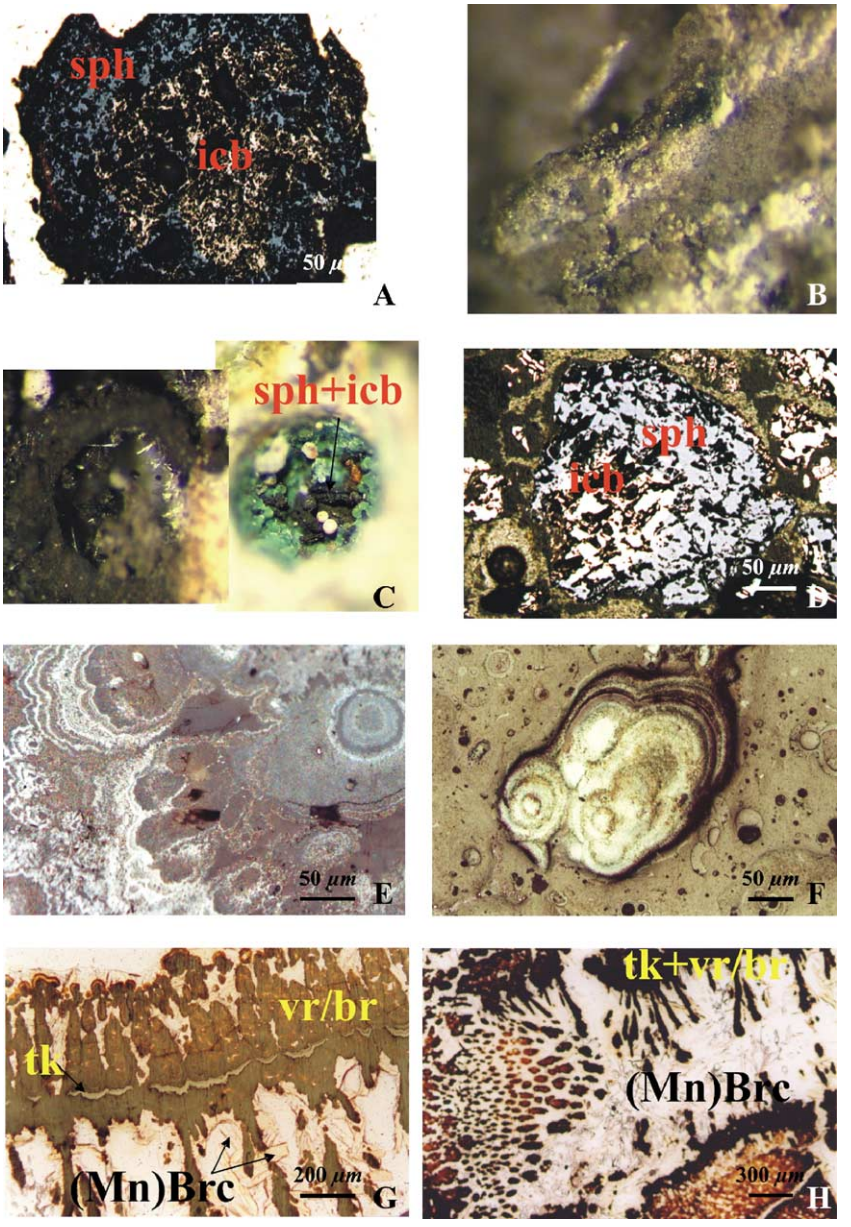

Fig. 4. Photomicrographs of polished sections from Mount Saldanha sediments samples; (A) polished section of isocubanite surrounded by sphalerite from SF13; (B) milimetric chimney at SF13. Outer walls are formed by cemented aggregates of manganese precipitates and carbonate and (C) inner walls are formed by manganese minerals, sulphides and a nonidentified green mineral. Some radiolarian tests were also identified inside these tubes; (D) polished section of isocubanite surrounded by sphalerite from a Rainbow sediment; (E–F) poorly crystalline Mn-oxides minerals. They are opaque showing a low relief and low reflectance with grey-brownish colours. They occur usually as collomorphic bands, and concretions comprise intimate mixtures of more crystalline and less crystalline manganese oxides, which seem to be todorokite and vernadite/birnesite, respectively. High reflectance bands, with whitish-grey colours, comprise the more crystalline specimen and low reflectance bands, with brownish-grey colours, comprise the poorly crystalline ones and are less well polished; (G–H) transparent fine crystals growing (Mn-brucite) into open spaces at poorly crystalline Mn-oxides. The right photomicrograph was taken in transmitted light conditions. icb = isocubanite; sph = sphalerite; tk = todorokite; vr/br = vernadite/birnesite; (Mn)Brc = Mn-brucite.

A strong negative correlation between MnO_2 and H_2O^+ was verified (Pearson's product-moment correlation coefficient: $r = -0.79$, $p < 0.001$, $n = 54$), which suggests that less crystalline specimens are more hydrated. The sample with the highest total was the one collected at the hydrothermal orifice (SF13),

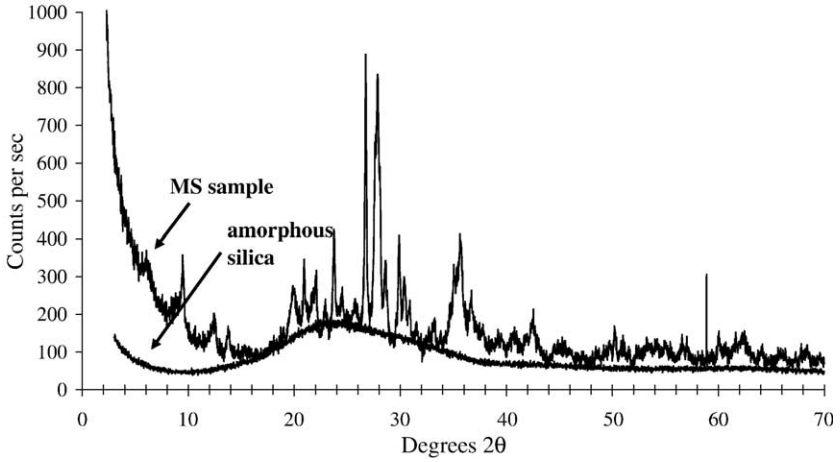

Fig. 5. X-ray diffractogram where two patterns have been superimposed: one from a sediment fine fraction (<4Φ fraction) and another from amorphous material. The elevation pattern at 25°, 2θ is due to the presence of amorphous material.

which reveals a strong substitution of Mn by Mg. This sample is clearly distinct from the remaining samples as a consequence of the Mg–Mn substitution in SF13 Mn-oxides and of the Fe–Mn substitution in the other MS and Rainbow sediments. Microprobe analyses revealed SiO_2 contents sometimes above 2%. This fact is consistent with previous chemical analyses for these minerals (e.g., Ostwald, 1988) and was also reported by Hekinian (1982) for FAMOUS samples. The abundance of Mg in minerals present in the SF13 sample is greater than those found at other locations mentioned before (e.g., Burns and Burns, 1978; Hoffert et al., 1978; Cronan, 1980; Roy, 1981; Ostwald, 1988).

In close association with Mn-oxide minerals in SF13 an uncommon and transparent mineral was identified (Fig. 4G and H). Chemical analyses of these crystals show an average of MnO and MgO wt.% of 22.6% and 41.6%, respectively, and low totals (range: 58.8–71.7%). The small size and scarcity of the crystals precluded an XRD investigation. The mineral is most probably manganobrucite, an extremely rare, poorly known variety of brucite, with ideal formula (Mg, Mn) $(OH)_2$.

Table 3
Chemical analyses of poorly crystalline Mn-oxides

	Mount Saldanha		SF13		Rainbow	
	Average	S.D.	Average	S.D.	Average	S.D.
SiO_2	1.27	1.37	2.34	4.17	1.06	0.38
Al_2O_3	0.42	0.38	0.10	0.07	0.12	0.12
MgO	1.55	1.77	13.98	7.59	0.44	0.12
Na_2O	0.82	1.10	0.08	0.09	0.05	0.04
MnO_2	49.29	15.88	53.86	14.48	41.23	15.30
V_2O_3	0.30	0.28	0.02	0.03	0.07	0.02
TiO_2	0.63	0.64	0.02	0.04	0.03	0.03
CaO	1.11	0.65	0.84	2.22	0.05	0.02
ZnO	0.05	0.03	0.03	0.02	0.03	0.04
NiO	0.25	0.55	0.01	0.01	0.01	0.01
FeO (T)	6.83	6.30	0.35	0.97	17.67	12.31
Cr_2O_3	0.01	0.01	0.01	0.02	0.02	0.01
Total	62.55	13.85	71.63	10.52	60.77	7.73
H_2O*	37.45		28.37		39.23	

The H_2O^+ percentage was assumed to be the difference from the total (100% − total).

3.2. Bulk sediment geochemistry

Bulk geochemical analyses (Appendix) show that MS sediments have high Ca and C concentrations. The highest concentrations of Ca (average = 37.6%) and C (average = 11.6%) were found in consolidated and semi-consolidated sediments and the lowest in the hydrothermal orifice sample SF13 (Ca = 28.7% and C = 9.1%). These Ca and C concentrations are in agreement with the samples' carbonate content estimated with the acid attack (Table 2).

The sediment collected at the hydrothermal orifice has high concentrations of Mn (3.2%) in comparison with the remaining MS samples (average Mn = 0.3%). Mg concentrations were highest in sample SF13 (4.2%) but also relatively high in samples SF10 (3.5%) and SF12 (1.7%) collected nearer the orifices, when compared with the remaining MS samples (0.7%). Rainbow sediments present higher values of Mg and Mn in comparison to the average of MS

sediments (average: Mg=1.7% and Mn=1.8%) but smaller than those recorded in the sediment collected at the hydrothermal orifice. The presence of these two elements is likely to be correlated with the occurrence of todorokite, vernardite and manganobrucite. Mg and Mn enrichment in hydrothermal sediments from other sediment-hosted systems has been reported (e.g., Koski et al., 1985; Goodfellow and Franklin, 1993; Usui et al., 1997). The enrichment in Mg is the result of unmodified seawater mixing with the hydrothermal system. The higher Mg enrichment in the three samples collected at the top of the mount suggests a more intense mixing of seawater with hydrothermal fluids in this area. In contrast, the Mn enrichment is derived from the hydrothermal fluids (e.g., Hodkinson and Cronan, 1995) and was most visible in the hydrothermal orifice sample (SF13).

Al_2O_3 concentration in MS sediments is low (average=1.05%) revealing a minor detrital component, as revealed by petrographic observations. The abundance of Al_2O_3 is generally strongly correlated with the abundance of SiO_2 in MS sediments ($r=0.97$; $N=14$; $p<0.001$) suggesting the same detrital origin for Al and Si. The Si/Al ratio is higher in the two samples collected nearer the orifices (SF10=4.71 and SF12=4.04), suggesting that some hydrothermal input of Si may have occurred in this particular area of the field. However, the Si/Al ratio in the SF13 sample collected in the orifice (2.06) did not differ from the remaining MS samples, which could be a consequence of Si precipitation at a greater depth. The presence of amorphous silica in MS samples revealed by XRD further supports some hydrothermal input of Si. Also, Rainbow sediments have a higher Si/Al ratio (average=18.8) consistent with a stronger input of hydrothermal Si.

Copper, Zn and Fe concentration is low in the MS samples, although the Fe+Cu+Zn concentration correlates with S ($r=0.66$; $N=14$; $p<0.01$). This is consistent with the small amounts of sulphide minerals observed and confirms that these metals are present as sulphides.

The sample collected at the vent had a concentration of U (0.75 ppm) higher than the remaining MS samples (average=0.44 ppm), although much lower than the Rainbow samples (average=9.46 ppm). The U in hydrothermal sediments is thought to be seawater-derived as hydrothermal fluids are stripped of dissolved U (e.g., Chen et al., 1986; James et al., 2003).

The enrichment in Co, Cr and Ni is likely to be due to the presence of ultramafic rocks in the sediments. Indeed, the Cr/Al and Ni/Al ratios are higher in sediments where larger amounts of ultramafic rocks were found (Table 1), reflecting the presence of an ultramafic component.

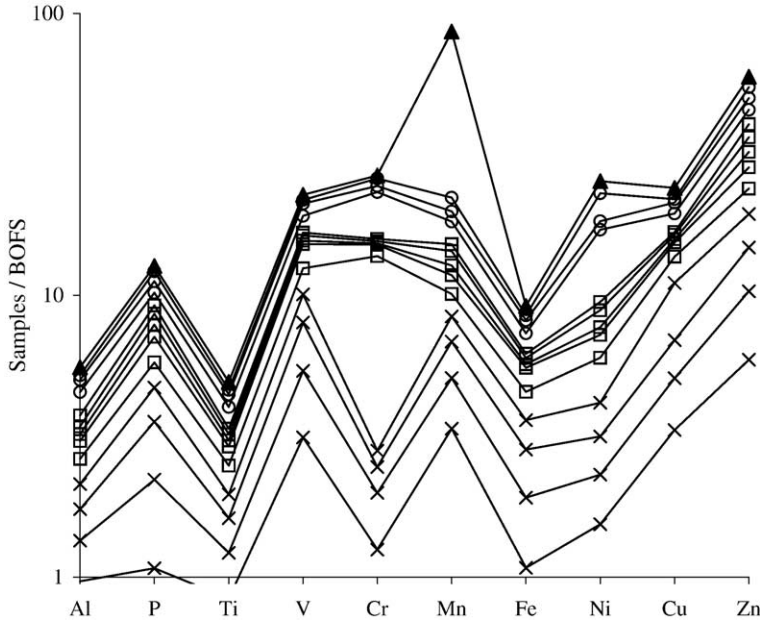

Fig. 6. Mount Saldanha sediment samples normalized to mean concentration of BOFS (Cave et al., 2002). Legend: ×–SF1, SF2, SF3, SF4; □–SF5, SF6, SF7, SF8, SF9; ○–SF10, SF11, SF12; ▲–SF13.

When MS sediments were normalised to non-hydrothermal pelagic sediments (BOFS), peaks at P, V, Mn, Fe, Cu and Zn were found (Fig. 6) due to enrichments caused by the hydrothermal component. Four different groups of samples can be distinguished: (a) the sediment collected in the hydrothermal orifice (SF13) has a clear hydrothermal signature and is particularly enriched in Mn; (b) sediments collected near the orifices (SF19, SF11, SF13) are very similar to SF13 but show a less pronounced Mn enrichment; and (c) and (d) sediments collected further away from the hydrothermal input are less enriched in Cr and Ni. The main difference between samples (c) and (d) is the lack of ultramafic rock fragments in the latter, with concomitant lower abundances in Cr and Ni (Table 1).

The hydrothermal vs. detrital contribution in sediments can be estimated using the Fe/Ti vs. Al/(Al+Fe+Mn) ratio (Boström, 1973). In this diagram, all hydrothermal sediments should lie on a theoretical curve. A decrease in the Fe/Ti ratio and an increase in the Al/(Al+Fe+Mn) ratio should indicate the dilution of metalliferous sediments with pelagic deep-sea ones. Boström (1973) also shows that the ratio Al/(Al+Fe+Mn) is generally above 0.4 in pelagic deep-sea sediments and that lower values indicate an enrichment in metals. Sample SF13 has a value of Al/(Al+Fe+Mn) below 0.4, revealing a strong hydrothermal component and an enrichment in Fe and Mn (Fig. 7). The remaining MS samples fall along the theoretical curve but show a marked detrital dilution. As expected, Rainbow sediments present a marked hydrothermal component with the lowest Al/(Al+Fe+Mn) values.

3.3. Rare-earth elements

Rare-earth element (REE) concentrations of all samples (Appendix) have been normalized to the chondrite values of Taylor and McLennan (1985). All MS samples, including SF13, show similar patterns (Fig. 8). They exhibit a depletion on HREE (heavy rare-earth elements) and negative Eu and Ce-anomaly (averages Ce/Ce*=0.61 and Eu/Eu*=0.73). REE patterns for Rainbow sediments also show a depletion of HREE with a strong positive Eu-anomaly (average Eu/Eu*=5.64, maximum Eu/Eu*=12.23) and a weak negative Ce-anomaly (average Ce/Ce*=0.57). Again, the REE values of the SR2 sample are clearly more alike to the MS ones (Ce/Ce*=0.61 and Eu/Eu*=1.00).

Comparing our REE data with seawater (Elderfield and Greaves, 1982), pelagic sediments (Wildeman and Haskin, 1965) and hydrothermal fluids (Douville et al., 2002), it is clear that MS sediments have a negative Ce anomaly, less pronounced than seawater, and lack a positive Eu anomaly like hydrothermal fluids, presenting instead a slightly negative Eu-anomaly as in seawater and pelagic sediments.

Rainbow sediments exhibit an average pattern very different from the seawater REE pattern and especially similar to the hydrothermal fluids pattern (negative Ce-anomaly and positive Eu-anomaly). The average MS REE pattern is similar to the pattern described for other sediments that contain hydrothermal precipitates (e.g., Toth, 1980; Courtois, 1981; Mills and Elderfield, 1993; Marchig et al., 1999). The absence of a positive Eu anomaly in MS samples can be explained as by Sverjensky (1984). This author concluded that at low temperatures (<250 °C),

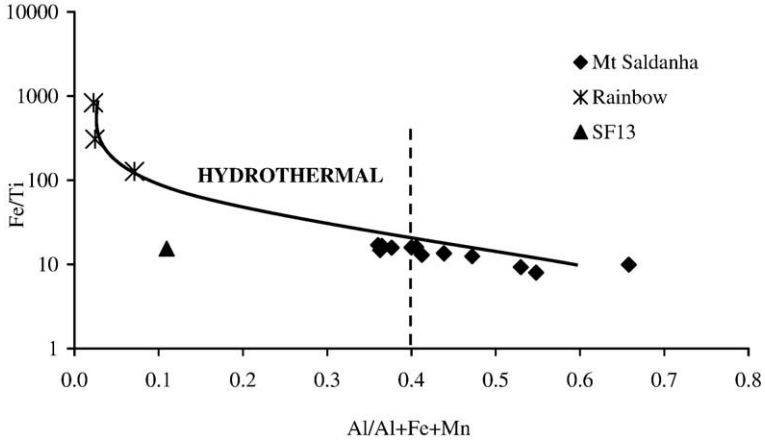

Fig. 7. Ratios Fe/Ti vs. Al/(Al+Fe+Mn) for Mount Saldanha and Rainbow sediments (adapted from Boström, 1973). It was not possible to project the ratios of the SR3 sample because the Ti concentration was below the threshold detection limit.

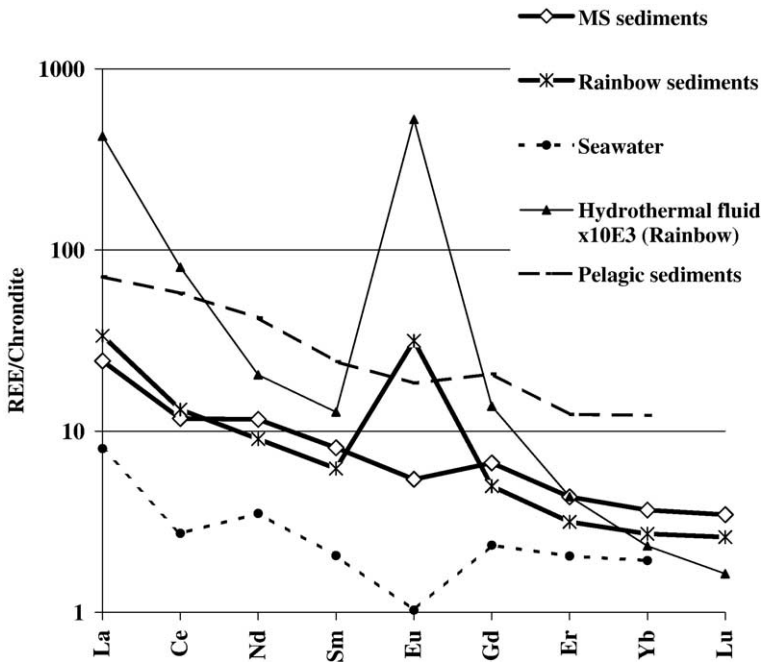

Fig. 8. Chondrite-normalized (Taylor and McLennan, 1985) average REE pattern for Mount Saldanha and Rainbow sediments. Also shown for comparison are (1) seawater patterns from 2500 m deep ($\times 10^4$) (Elderfield and Greaves, 1982); (2) pelagic sediments (Wildeman and Haskin, 1965); and (3) hydrothermal fluids ($\times 10^3$) from Rainbow (Douville et al., 2002).

the geochemistry of Eu should be dominated by the trivalent stage, like all of REEs, and consequently, Eu should not exhibit a positive anomaly. In contrast, the predicted stability of divalent Eu at elevated temperatures is consistent with the large positive Eu anomalies in REE patterns. Michard (1989) also shows that hydrothermal fluids below 250 °C are characterized by negative Eu anomalies, in agreement with the low temperature of the fluids measured at MS hydrothermal orifices (<9 °C). However, the possibility remains that at greater depths, the fluids are warmer, cooling down when mixing with unmodified seawater nearer the surface. The REE patterns of MS sediments clearly show that seawater and the dominant pelagic fraction overprint the REE hydrothermal signature.

4. Conclusions

The Mount Saldanha hydrothermal field is a serpentinite-hosted system covered by sediments in which the hydrothermal activity is mainly diffuse with some focused discharge occurring along centimetric vents at the top of the mount. The mineralogical and geochemical data from MS sediments suggest an environment of deposition with percolation of hydrothermal fluids through pelagic sediments. The hydrothermal component is strongly "diluted" in pelagic carbonate ooze and is dominated by early sulphides, nontronite, smectites, poorly crystallized Mn oxyhydroxides and amorphous material, which probably precipitated from a reduced and mildly acid circulating hydrothermal fluid, under low-temperature conditions.

The REE patterns of MS sediments have a fingerprint of seawater with negative anomalies of Ce and Eu, and the resemblance with pelagic sediments reflects the strong dilution of the hydrothermal component in the carbonate ooze. In contrast, Rainbow sediments REE patterns show a strong contribution of the high-temperature hydrothermal fluids.

The mineralogy and chemistry of the sediments suggest that the hydrothermal contribution is particularly intense near the discharge hydrothermal fluid orifices. Here, micro-chimneys composed mainly of sphalerite and isocubanite in a concentric arrangement were identified.

At the discharge zone, the concentration of Mn and Mg is particularly high, and poorly crystalline Mn–Mg oxyhydroxides and putative manganobrucite were identified. The Mg enrichment, together with the occurrence of sulphide minerals, may be explained by the interaction between seawater percolating down into the sediments and the upwelling

modified seawater. The sulphides are likely to precipitate from the modified seawater at larger depths, whereas Mg precipitates when extensive interaction with cold, unmodified seawater occurs.

The slight enrichment of MS sediments in Al and Si is probably due to detrital lithic inclusions, although the higher Si/Al ratio in SF10 and SF12 samples and the presence of amorphous silica suggest a hydrothermal input in places.

In comparison to background pelagic sediments, MS sediments are also enriched in P, V, Fe, Cu and Zn, precipitated from hydrothermal fluids. Some MS sediments are also particularly enriched in Ni and Cr, derived from ultramafic fragments such as serpentinites and steatites.

The mineralogy of the sediments, in particular the occurrence of sulphides, suggests higher temperatures for this system than the ones measured at the vents (6–9 °C). Thus, the low temperature of MS fluids at the discharge orifices may reflect the effects of cooling during convective circulation, with consequent seafloor alteration, and seawater mixing.

This study revealed a metal enrichment in the sediments, especially at the top of the mount. Although sediment-hosted hydrothermal systems are rare along the Mid-Atlantic Ridge, many of the word's largest massive sulphide ore deposits appear to have originated in similar depositional environments. The precipitation of hydrothermal minerals seems to occur inside sediments where an oxidized cap prevents the direct contact of the evolved hydrothermal fluid with the oxidizing unmodified seawater. Similar caps were postulated for the formation of sub-seafloor massive sulphide mineralizations, both modern (e.g., Bent Hill, Zierenberg et al., 1998) and fossil (e.g., Aljustrel deposits, Iberian Pyrite Belt, Barriga, 1983; Barriga and Fyfe, 1988).

Mount Saldanha and Rainbow sediments, in spite of occurring in similar geological settings, are influenced by fluids putatively of different temperatures, which results in a distinct suite of mineral and geochemical signatures. The Mount Saldanha hydrothermal system seems to be of lower temperature and the lack of a magmatic heat source, the presence of altered peridotite to serpentinites and steatites (talc rock) and the occurrence of a strong methane anomaly within the overlying water column, agree with the system being driven exclusively by heat released during the serpentinization process. In contrast, an additional heat source seems to be required to explain the much hotter Rainbow system (Lowell and Rona, 2002; Allen and Seyfried, 2004). Nevertheless, additional geophysical and geochemical data are needed to understand the heat sources of these systems.

Acknowledgements

We thank all the participants in the SALDANHA'98 cruise (Nadir-Nautile) for various forms of indispensable cooperation in surveying and sampling Mount Saldanha. In particular, we thank Yves Fouquet for sharing with us his experience in seafloor studies. CREMINER researchers and technicians, especially Patrícia Conceição, Carlos Carvalho, Raquel Costa and Alberto Verde are most gratefully thanked for various forms of cooperation, ranging from thin-section preparation and X-ray diffraction work to frequent and enlightening discussions. We also thank Martin Sinha, Michelle Ellis and Cândida Shinn for reviewing the English of the manuscript. We acknowledge financial support from FCT (Portugal) through projects AMAR-Praxis XXI no. 2/2.1/MAR/1743/95 and SEAHMA PDCTM/P/MAR/15281/1999 and through an MSc scholarship to the senior author. This paper has benefited from reviews by G. J. de Lange, G. P. Glasby and an anonymous reviewer.

Appendix A. Chemical composition of samples from Mount Saldanha and Rainbow

	Method	Detection limit	SF 1	SF 2	SF 3	SF 4	SF 5	SF 6	SF 7	ST 8	SF 9	SF 10	SF 11	SF 12	SF 13	SF14
Mount Saldanha																
SiO_2	ICP	0.01%	6.84	2.72	2.94	2.90	3.72	3.05	1.33	1.82	2.20	10.39	3.51	2.06	2.05	3.11
Al_2O_3	ICP	0.01%	2.39	0.94	0.98	0.98	1.21	1.02	0.44	0.51	0.80	1.95	1.19	0.45	0.88	1.01
Fe_2O3	ICP	0.01%	2.73	2.11	2.33	1,95	2.37	2.50	0.41	0.76	0.51	2.86	2.08	0.86	1.68	2.04
MnO	ICP	0.001	0.217	0.111	0.114	0.101	0.109	0.108	0.063	0.103	0.054	0.299	0.102	0.155	4.131	0.114
MgO	ICP	0.01%	1.23	0.57	0.60	0.64	0.78	0.67	0.43	0.66	0.93	3.50	0.86	1.66	6.97	0.91
CaO	ICP	0.01%	44.41	49.83	43.73	49.26	48.43	49.37	53.71	52.31	52.51	42.30	48.97	51.88	40.22	49.40
Na_2O	ICP	0.01%	2.06	1.32	1.40	1.74	1.48	1.48	0.96	1.11	0.64	1.53	1.39	0.46	1.37	1.42
K_2O	ICP	0.01%	0.20	0.14	0.18	0.19	0.20	0.17	0.13	0.14	0.17	0.14	0.18	0.11	0.11	0.17
TiO_2	ICP	0.005%	0.172	0.078	0.082	0.071	0.107	0.086	0.030	0.033	0.030	0.134	0.089	0.034	0.064	0.075
P_2O5	ICP	0.01%	0.16	0.17	0.20	0.17	0.16	0.20	0.11	0.11	0.09	0.15	0.15	0.14	0.08	0.16
LOI	ICP	0.01%	38.85	42.78	47.55	42.95	41.89	42.30	43.17	43.13	42.49	36.15	41.81	42.34	40.86	42.52
Total			99.27	100.78	100.09	100.93	100.45	100.95	100.78	100.69	100.43	99.30	100.33	100.14	98.42	100.91
CO_2	IR	0.05%	35.50	40.50	39.50	40.00	39.00	39.50	43.00	41.80	42.50	34.50	38.00	43.50	33.00	40.00
SO_4	IR	0.05%	0.20	0.20	0.25	0.20	0.20	0.20	0.10	0.15	0.10	0.25	0.15	0.10	0.30	0.10
C	LECO	0.01%	9.80	11.10	11.90	11.00	10.70	10.90	11.70	11.40	11.60	9.75	10.10	11.80	9.10	11.00
S	LECO	0.01%	0.11	0.09	0.11	0.10	0.09	0.09	0.05	0.06	0.04	0.11	0.08	0.04	0.13	0.07
Sc	ICP	0.01 ppm	6.30	1.80	1.80	1.70	2.00	1.90	1.10	1.40	1.70	4.20	2.70	2.30	1.80	2.30
V	ICP	5 ppm	97	70	81	64	74	85	13	21	12	76	62	20	29	66
Cr	ICP	0.5 ppm	28.8	16.9	10.8	8.1	252.0	31.2	3.4	6.4	6.4	170.0	27.5	35.5	14.9	23.9
Co	ICP	0.1 ppm	35.7	13.8	12.1	13.4	15.4	13.0	6.0	12.7	11.8	23.7	13.8	38.3	14.0	14.7
Ni	ICP	1 ppm	20	10	11	13	24	16	6	15	8	99	16	61	31	22
Cu	ICP	1 ppm	133	70	74	165	106	68	16	24	14	110	72	25	84	62
Zn	ICP	1 ppm	124	93	93	98	94	95	80	86	86	106	96	98	102	101
Ga	ICP/MS	1 ppm	2.0	1.0	1.2	1.2	1.3	1.3	nd	nd	nd	2.0	1.8	nd	10.9	3.5
Ge	ICP/MS	0.5 ppm	0.6	3.8	nd	nd	nd	0.6	nd	nd	nd	0.8	nd	nd	nd	nd
As	ICP	1 ppm	39	37	40	32	37	44	5	8	5	29	30	11	11	32
Br	ICP	0.5 ppm	90.0	69.9	75.6	90.0	72.8	79.8	44.9	51.5	25.2	63.3	68.7	20.2	115.0	71.9
Rb	ICP/MS	2 ppm	3.0	3.1	3.2	3.7	3.8	3.6	2.0	2.3	3.4	3.0	3.7	nd	3.2	3.9
Sr	ICP	2 ppm	1384	1504	1482	1488	1456	1544	1515	1491	1188	1277	1396	1235	1169	1443
Y	ICP	1 ppm	15	12	13	12	12	13	10	13	12	11	11	17	10	11
Zr	ICP	4 ppm	25	23	22	22	28	24	13	15	17	23	23	14	14	20
Nb	ICP/MS	2 ppm	3.4	3.4	3.2	3.0	3.6	3.3	1.6	1.7	2.8	3.2	3.0	2.2	2.5	2.9
Mo	INAA	2 ppm	2	nd	nd	nd	nd	nd	nd	2	nd	nd	nd	nd	nd	nd
Pb	ICP	5 ppm	13	nd	nd	nd	nd	11	nd	nd	nd	nd	nd	nd	6	nd
Ag	ICP	0.4 ppm	0.5	0.5	0.4	0.5	0.5	0.5	0.5	0.5	0.5	0.4	0.4	0.5	nd	0.5
Cd	ICP	0.5 ppm	nd	nd	nd	nd	nd	nd	0.5	0.5	0.9	nd	nd	1.3	0.6	nd
Sn	ICP/MS	1 ppm	3	nd	nd	nd	nd	2	nd	nd	nd	nd	nd	nd	nd	nd
Sb	INAA	0.1 ppm	0.5	0.5	0.5	0.4	0.5	0.6	0.1	0.3	0.2	0.5	0.4	0.5	0.2	0.5
Cs	ICP	0.1 ppm	0.1	0.2	0.2	0.2	0.2	0.2	0.1	0.1	0.2	0.2	0.2	nd	0.2	0.2
Ba	ICP	1 ppm	174	163	171	154	117	156	13	24	16	147	136	16	110	132
La	ICP/MS	0.05 ppm	10.50	9.41	9.80	8.83	10.30	9.96	6.50	8.14	8.17	8.24	8.28	10.95	7.93	8.35
Ce	ICP/MS	0.1 ppm	16.3	12.3	12.5	11.4	13.3	12.9	6.4	8.0	9.2	11.5	10.8	12,0	9.9	10.8
Pr	ICP/MS	0.02 ppm	2.24	2.03	2.07	1.94	2.24	2.16	1.41	1.74	1.69	1.72	1.77	2.25	1.70	1.80
Nd	ICP/MS	0.05 ppm	9.65	8.79	9.11	8.00	9.28	9.18	6.39	7.68	7.41	7.47	7.74	10.00	7.32	7.61
Sm	ICP/MS	0.01 ppm	2.23	1.96	2.09	1.71	2.03	1.98	1.40	1.69	1.61	1.92	1.69	2.24	1.96	1.69
Eu	ICP/MS	0.005 ppm	0.598	0.481	0.513	0.454	0.531	0.508	0.364	0.487	0.375	0.454	0.441	0.574	0.400	0.425

(continued on next page)

Appendix A (*continued*)

Gd	ICP/MS	0.02 ppm	2.46	2.06	2.17	1.91	2.13	2.24	1.67	1.99	1.79	1.95	1.80	2.64	1.83	1.96
Tb	ICP/MS	0.01 ppm	0.40	0.34	0.34	0.30	0.36	0.35	0.25	0.33	0.28	0.29	0.30	0.43	0.27	0.30
Dy	ICP/MS	0.02 ppm	2.43	1.91	1.94	1.80	1.99	1.97	1.49	1.82	1.64	1.72	1.64	2.57	1.55	1.69
Ho	ICP/MS	0.01 ppm	0.48	0.38	0.40	0.36	0.39	0.41	0.31	0.38	0.35	0.35	0.34	0.54	0.32	0.35
Er	ICP/MS	0.01 ppm	1.37	1.06	1.08	0.96	1.12	1.16	0.82	1.10	1.01	1.03	0.98	1.52	0.89	1.00
Tm	ICP/MS	0.005 ppm	0.192	0.151	0.156	0.144	0.155	0.159	0.114	0.154	0.148	0.150	0.141	0.221	0.128	0.146
Yb	ICP/MS	0.01 ppm	1.22	0.90	0.94	0.82	0.96	0.94	0.66	0.93	0.83	0.86	0.82	1.24	0.78	0.84
Lu	ICP/MS	0.05 ppm	0.18	0.13	0.13	0.12	0.13	0.14	0.10	0.13	0.13	0.13	0.12	0.19	0.11	0.12
Hf	ICP/MS	0.01 ppm	0.60	0.44	0.47	0.45	0.60	0.49	0.26	0.31	0.43	0.50	0.48	0.33	0.39	0.42
Ta	ICP/MS	0.1 ppm	0.20	0.21	0.22	0.20	0.25	0.22	nd	nd	0.20	0.20	0.21	nd	0.16	0.19
Au	INAA	2 ppb	9	5	7	5	15	7	nd	nd	nd	8	3	nd	4	6
Hg	INAA	1 ppm	nd	nd	nd	nd	nd	nd	nd	nd	nd	nd	nd	nd	nd	nd
Tl	ICP/MS	0.05 ppm	0.05	0.09	0.08	0.06	nd	0.08	0.07	0.10	0.08	0.15	0.06	0.33	0.06	0.10
Bi	ICP/MS	0.06 ppm	nd	nd	0.11	nd	0.06	0.07	0.07	0.08	nd	0.11	0.09	0.18	0.26	0.09
Th	ICP/MS	0.05 ppm	1.27	1.14	1.19	1.11	1.31	1.22	0.55	0.62	0.83	0.99	1.03	0.84	0.97	1.01
U	ICP/MS	0.05 ppm	0.52	0.43	0.46	0.43	0.47	0.48	0.40	0.46	0.35	0.39	0.40	0.49	0.75	0.42
Si/Al			2.53	2.56	2.65	2.61	2.72	2.64	2.67	3.15	2.43	4.71	2.61	4.04	2.06	2.72

	Method	Detection limit	SR 1	SR 2	SR 3	SR 5
Rainbow						
SiO_2	ICP	0.01%	4.66	8.40	0.95	4.87
Al_2O_3	ICP	0.01%	1.01	1.11	0.04	0.61
Fe_2O_3	ICP	0.01%	44.34	18.52	52.58	39.88
MnO	ICP	0.001%	7.665	1.518	0.015	0.041
MgO	ICP	0.01%	3.95	4.53	0.25	1.57
CaO	ICP	0.01%	7.96	29.47	0.20	0.93
Na_2O	ICP	0.01%	0.12	0.09	0.75	0.53
K_2O	ICP	0.01%	0.03	0.03	0.02	0.17
TiO_2	ICP	0.005%	0.084	0.085	nd	0.028
P_2O_5	ICP	0.01%	0.44	0.30	0.14	0.64
LOI	ICP	0.01%	23.98	34.12	27.46	26.71
Total			94.24	98.17	82.41	75.98
CO2	IR	0.05%	8.90	28.50	0.48	3.60
SO4	IR	0.05%	0.30	0.35	2.30	0.15
C	LECO	0.01%	2.54	8.00	0.24	1.15
S	LECO	0.01%	0.24	0.29	>25.00	5.00
Sc	ICP	0.01 ppm	2.30	2.70	0.20	0.80
V	ICP	5 ppm	204	136	100	294
Cr	ICP	0.5 ppm	94.8	405.0	13.3	115.0
Co	ICP	0.1 ppm	290.0	78.3	2810.0	952.0
Ni	ICP	1 ppm	175	185	15	96
Cu	ICP	1 ppm	22,815	2049	91,645	>99,999
Zn	ICP	1 ppm	4107	554	30,162	10,270

Ga	ICP/MS	1 ppm	17.66	10.96	19.47	13.89
Ge	ICP/MS	0.5 ppm	1.58	1.06	2.32	5.94
As	ICP	1 ppm	90	56	115	244
Se	ICP	0.5 ppm	8.0	nd	41.5	103.0
Br	ICP	0.5 ppm	44.9	68.8	39.7	99.2
Rb	ICP/MS	2 ppm	3,0	5.1	nd	2.4
Sr	ICP	2 ppm	485	965	621	391
Y	ICP	1 ppm	13	12	nd	6
Zr	ICP	4 ppm	16	22	8	10
Nb	ICP/MS	2 ppm	3.12	2.89	0.87	1.27
Mo	INAA	2 ppm	110	7	66	90
Pb	ICP	5 ppm	53	22	193	150
Ag	ICP	0.4 ppm	3.8	0.6	62.1	53.5
Cd	ICP	0.5 ppm	5.5	1.5	89.4	18.3
In	ICP/MS	0.1 ppm	0.63	0.12	1.25	4.05
Sn	ICP/MS	1 ppm	32	2	nd	63
Sb	INAA	0.1 ppm	4.2	1.2	9.9	10.5
Cs	ICP	0.1 ppm	0.2	0.3	0.2	0.1
Ba	ICP	1 ppm	3159	1757	12,937	8318
La	ICP/MS	0.05 ppm	14.20	10.71	6.78	17.62
Ce	ICP/MS	0.1 ppm	15.9	12.9	5.8	15.8
Pr	ICP/MS	0.02 ppm	2.44	2.04	0.47	1.41
Nd	ICP/MS	0.05 ppm	10.21	8.87	1.69	4.97
Sm	ICP/MS	0.01 ppm	2.26	1.91	0.59	1.00
Eu	ICP/MS	0.005 ppm	6.930	0.668	2.090	1.300
Gd	ICP/MS	0.02 ppm	2.44	2.19	0.42	1.04
Tb	ICP/MS	0.01 ppm	0.39	0.33	0.06	0.16
Dy	ICP/MS	0.02 ppm	2.17	1.90	0.26	0.91
Ho	ICP/MS	0.01 ppm	0.45	0.39	0.05	0.19
Er	ICP/MS	0.01 ppm	1.33	1.10	0.16	0.55
Tm	ICP/MS	0.005 ppm	0.183	0.152	0.025	0.075
Yb	ICP/MS	0.01 ppm	1.06	0.96	0.18	0.49
Lu	ICP/MS	0.05 ppm	0.15	0.14	0.03	0.08
Hf	ICP/MS	0.01 ppm	0.55	0.49	0.15	0.19
Ta	ICP/MS	0.1 ppm	0.23	0.21	nd	nd
W	ICP/MS	0.20 ppm	1.67	0.24	3.85	4.36
Au	INAA	2 ppb	853	217	5870	9030
Hg	INAA	1 ppm	nd	nd	nd	nd
Tl	ICP/MS	0.05 ppm	0.63	nd	0.20	0.07
Bi	ICP/MS	0.06 ppm	3.22	0.08	0.33	24.92
Th	ICP/MS	0.05 ppm	1.24	1.10	nd	0.31
U	ICP/MS	0.05 ppm	7.87	1.43	12.43	16.13
Si/Al			9.52	2.20	55.35	8.19

References

Allen, D.E., Seyfried Jr., W.E., 2003. Compositional controls on vent fluids from ultramafic-hosted hydrothermal systems at mid-ocean ridges: an experimental study at 400 °C, 500 bars. Geochim. Cosmochim. Acta 67 (8), 1531–1542.

Allen, D.E., Seyfried Jr., W.E., 2004. Serpentinization and heat generation: constraints from Lost City and Rainbow hydrothermal systems. Geochim. Cosmochim. Acta 68 (6), 1347–1354.

Alt, J.C., 1988. Hydrothermal oxide and nontronite deposits on seamounts in the Eastern Pacific. Mar. Geol. 81, 227–239.

Ames, D.E., Franklin, J.M., Hannington, M.D., 1993. Mineralogy and geochemistry of active and inactive chimneys and massive sulfide, middle valley, northern Juan de Fuca Ridge: an evolving hydrothermal system. Can. Mineral. 31, 997–1024.

Aoki, S., Kohyamab, N., Hotta, H., 1996. Hydrothermal clay minerals found in sediment containing yellowish-brown material from the Japan Basin. Mar. Geol. 129 (3–4), 331–336.

Bach, W., Banerjee, N.R., Dick, H.J.B., Baker, E.T., 2002. Discovery of ancient and active hydrothermal systems along the ultra-slow spreading Southwest Indian Ridge 10°–16°E. Geochem. Geophys. Geosyst. 3 (7).

Barriga, F.J.A.S., 1983. Hydrothermal metamorphism and ore genesis at Aljustrel, Portugal. PhD thesis, University of Western Ontario, Ontario. 368 pp.

Barriga, F.J.A.S., Fyfe, W.S., 1988. Giant pyritic base-metal deposits: the example of Feitais (Aljustrel, Portugal). Chem. Geol. 69, 331–343.

Barriga, F.J.A.S., Teem, Seahma, 2003. Seahma-1 Cruise Report, FCT, Portugal, July–August 2002, Creminer. Faculty of Sciences University of Lisbon, Lisbon.

Barriga, F.J.A.S., Fouquet, Y., Almeida, A., Biscoito, M., Charlou, J.-L., Costa, R.P.C., Dias, A., Marques, A.M.S.F., Miranda, J.M.A., Olu, K., Porteiro, F., Queiroz, P.S., 1998. Discovery of the Saldanha hydrothermal field on the famous segment of the MAR (36° 30′N). AGU-Fall Meeting, Eos. Trans, vol. 79 (45), pp. F67.

Bischof, J.L., 1972. A ferroan nontronite from the Red Sea geothermal system. Clays Clay Miner. 20, 217–223.

Bogdanov, Y.A., Bortnikov, N.S., Vikentev, I.V., Gurvich, E.G., Sagalevich, A.M., 1997. New type of the modern mineral-forming system: black smokers of the hydrothermal field 14°45′N MAR. Geol. Ore Depos. 39 (1), 58–78.

Bonatti, E., Fisher, D.E., Joensuu, O., Ridell, H.S., Benty, M., 1972. Iron–manganese–barium deposits from the northern Afar Rift (Ethiopia). Econ. Geol. 67 (6), 717–730.

Boström, K., 1973. The origin and fate of ferromanganoan active ridge sediments. Stockh. Contrib. Geol. 27, 149–243.

Bougault, H., Aballéa, M., Radford-Knoery, J., Charlou, J.-L., Baptiste, P., Appriou, J., Needham, P., German, D., Miranda, C., 1998. FAMOUS and AMAR segments on the Mid-Atlantic Ridge: ubiquitous hydrothermal Mn, CH4, delta ^{3}He signals along the rift valley walls and rift offsets. Earth Planet. Sci. Lett. 161, 1–17.

Burns, V.M., Burns, R.G., 1978. Post-depositional metal enrichment processes inside manganese from the north Equatorial Pacific. Earth Planet. Sci. Lett. 39, 341–348.

Cave, R.R., German, C.R., Thomson, J., Nesbitt, R.W., 2002. Fluxes to sediments underlying the rainbow hydrothermal plume at 36°14′N on the Mid-Atlantic Ridge. Geochim. Cosmochim. Acta 66 (11), 1905–1923.

Charlou, J.-L., Bougault, H., Donval, J., Pellé, P.H., Langmuir, C., Team, F.S., 1993. Seawater CH4 concentration over the Mid-Atlantic Ridge from the Hayes F.Z. to the Azores triple junction. Eos 74, 380.

Charlou, J.-L., Donval, J.-P., Douville, E., Knoery, J., Fouquet, Y., Bougault, H., Baptiste, P., Stievenard, M., German, C., 1997. High methane flux between 15°N and the Azores Triple Junction, Mid-Atlantic ridge, hydrothermal and serpentinization processes. Eos Trans. AGU 78 (F831).

Chen, J.H., Wasserburg, G.J., von Damm, K.L., Edmond, J.M., 1986. The U–Th–Pb systematics in hot springs on the East Pacific Rise at 21°N and Guaymas Basin. Geochim. Cosmochim. Acta 50 (11), 2467–2479.

Costa, R., 2001. Estudo mineralógico e geoquímico da alteração hidrotermal das rochas vulcânicas e ultramáficas serpentinizadas do Monte SALDANHA (RMA, Segmento FAMOUS /AMAR). MSc thesis, Faculdade de Ciências da Universidade de Lisboa, Lisboa, p. 142.

Courtois, C., 1981. Distribuition des Terres Rares dans les depots hydrothermaux de la zone FAMOUS et des Galapagos—comparation avec les sediments metalliferes. Mar. Geol. 39, 1–14.

Cronan, D.S., 1980. Underwater Minerals. Academic Press, London, p. 362.

Deer, W.A., Howie, R.A., Zussman, J., 1982. The Rock Forming Minerals. Longman Scientific & Technical, p. 696.

Detrick, R.S., Needham, H.D., Renard, V., 1995. Gravity anomalies and crustal thickness variation along Mid-Atlantic Ridge between 33°N and 40°N. J. Geophys. Res. 100, 3767–3787.

Douville, E., Charlou, J.-L., Oelkers, E., Bienvenu, H., Jove Colon, P., Donval, F., Fouquet, P., Prieur, Y., Appriou, D., 2002. The Rainbow vent fluids (36°14′N, MAR): the influence of ultramafic rocks and phase separation on trace metal content in Mid-Atlantic Ridge hydrothermal fluids. Chem. Geol. 184 (1–2), 37–48.

Elderfield, H., Greaves, M.J., 1982. The rare earth elements in seawater. Nature 18, 214–219.

Fouquet, Y., Wafik, A., Cambon, P., Mevel, C., Meyer, G., Gente, P., 1993. Tectonic setting and mineralogical and geochemical zonation in the snake pit sulfide deposit (Mid-Atlantic Ridge at 23°N). Econ. Geol. 88 (8), 2018–2036.

Fouquet, Y., Charlou, J.-L., Ondréas, H., Radford-Knoery, J., Donval, J.-P., Douville, E., Apprioual, R., Cambon, P., Pellé, H., Landuré, J.Y., Normand, A., Ponsevera, E., German, C., Parson, L., Barriga, F.J.A.S., Costa, I.M.A., Relvas, J.M.R., Ribeiro, A., 1997. Discovery and first submergible investigations on the Rainbow hydrothermal field on the MAR (36° 14N). Eos Trans. AGU 78 (F832).

Fouquet, Y., Barriga, F.J.A.S., Charlou, J.-L., Elderfield, H., German, C.R., Ondréas, H., Parson, L., Radford-Knoery, J., Relvas, J.M., Ribeiro, A., Schultz, A., Apprioual, R., Cambon, P., Costa, I., Donval, J.P., Douville, E., Landuré, J.Y., Normand, A.m., Pellé, H., Ponseveras, E., Riches, S., Santana, H., Stephan, M., 1998. FLORES diving cruise with the Nautile near Azores—first dives on rainbow field: hydrothermal seawater/mantle interaction. InterRidge News 7 (1), 1998.

Fyfe, W.S., 1974. Heat of chemical reactions and submarine heat production. Geophys. J. R. Astron. Soc. 37, 213–315.

German, C.R., Parson, L.M., Scientific Party of RRS, 1994. Charles Darwin cruise CD89, HEAT, hydrothermal exploration at the Azores Triple-Junction. Eos 75, 308.

German, C.R., Barreiro, B.A., Higgs, N.C., Nelsen, T.A., Ludford, E.M., Palmer, M.R., 1995. Seawater-metasomatism in hydrothermal sediments (Escanaba Trough, northeast Pacific). Chem. Geol. 119 (1–4, 5), 175–190.

German, C.R., Parson, L.M., HEAT Scientific Team, 1996. Hydrothermal exploration near the Azores Triple Junction: tectonic

control of venting at slow-spreading ridges? Earth Planet. Sci. Lett. 138, 93–104.
German, C.R., the FLAME Scientific Party, 1997. FLAME: the Fluxes at AMAR Experiment (AMORES) (abstract of paper presented at: AGU Fall Meeting, San Francisco, 8–12 Dec 1997). Eos. Trans. AGU 78 (46), F831 (Suppl).
Goodfellow, D., Franklin, J.M., 1993. Geology, mineralogy, and chemistry of sediment-hosted clastic massive sulfides in shallow cores, middle valley, Northern Juan de Fuca Ridge. Econ. Geol. 88 (8), 2037–2068.
Gràcia, E., Charlou, J.-L., Radford-Knoery, J., Parson, L., 2000. Non-transform offset along the Mid-Atlantic ridge south of the Azores (38°N–34°N): ultramafic exposures and hosting of hydrothermal vents. Earth Planet. Sci. Lett. 177, 89–103.
Hannington, M.D., Jonasson, I.R., Herzig, P.M., Peterson, S., 1995. Physical and chemical processes of seafloor mineralization at Mid-Ocean Ridge. In: Humphris, S., Fornari, D., Zierenherg, R. (Eds.), Physical, Chemical, Biological, and Geological Interactions within Hydrothermal Systems, Am. Geophys. Union Monogr., vol. 91, pp. 115–157.
Harder, H., 1976. Nontronite synthesis at low temperatures. Chem. Geol. 18, 169–180.
Haymon, R.M., 1983. Growth history of black smokers hydrothermal chimney. Nature 301, 695–698.
Haymon, R.M., Kastner, M., 1981. Hot spring deposits on the East Pacific Rise at 21°N: preliminar description of mineralogy and genesis. Earth Planet. Sci. Lett. 53, 363–381.
Hekinian, R., 1982. Petrology of the Ocean Floor. Elsevier Scientific Publishing Company, Amsterdam, p. 393.
Hékinian, R., Hoffert, M., Larque, P., Cheminée, J.L., Stoffers, P., Bideau, D., 1993. Hydrothermal Fe and Si oxyhydroxide deposits from South Pacific intraplate volcanoes and East Pacific Rise axial and off-axial regions. Econ. Geol. 88, 2099–2121.
Hodkinson, R.A., Cronan, D.S., 1995. Hydrothermal sedimentation at ODP sites 834 and 835 in relation to crustal evolution of the Lau Backarc Basin. In: Parson, L.M., Walker, C.L., Dixon, D.R. (Eds.), Hydrothermal Vents and Processes. Geol. Sot., vol. 87. Spec. Publ., London, pp. 231–248.
Hoffert, M., Perseil, A., Hekinian, R., Choukroune, P., Needham, H.D., Francheteau, J., Le Pichon, X., 1978. Hydrothermal deposits sampled by diving saucer in Transform Fault "A" near 37° on the Mid-Atlantic ridge, FAMOUS area. Oceanol. Acta 1, 73–86.
James, R.H., Allen, D.E., Seyfried Jr., W.E., 2003. An experimental study of alteration of oceanic crust and terrigenous sediments at moderate temperatures (51 to 350[deg]C): insights as to chemical processes in near-shore ridge-flank hydrothermal systems. Geochim. Cosmochim. Acta 67 (4), 681–691.
Kelley, D.S., Karson, J.A., Blackman, D.K., Früh-Green, G.L., Butterfield, D.A., Lilley, M.D., Olson, E.J., Schrenk, M.O., Roe, K.K., Lebon, G.T., Rivizzigno, P., At3-60 Shipboard Party, 2001. An off-axis hydrothermal vent field near the Mid-Atlantic Ridge at 30°N. Nature 412, 445–449.
Koeppenkastrop, D., De Carlo, E.H., 1992. Sorption of rare-earth elements from seawater onto synthetic mineral particles: an experimental approach. Chem. Geol. 95, 251–263.
Koski, R.A., Lonsdale, P.F., Shanks, W.C., Berndt, M., Howe, S.S., 1985. Mineralogy and geochemistry of a sediment-hosted hydrothermal sulfide deposit from the Southern Trough of Guaymas Basin, Gulf of California. J. Geophys. Res. 90 (B8), 6695–6707.
Lafitte, M., Maury, R., Perseil, E.A., Boulegue, J., 1985. Morphological and analytical study of hydrothermal sulfides from 21° north East Pacific Rise. Earth Planet. Sci. Lett. 73, 53–64.
Langmuir, C., Klinkhammer, G., Bougault, H., Bourdon, B., Charlou, J.L., Chin, C., Conard, B., Desonie, D., Donval, J.P., Ferguson, E., Hirose, K., Mandal, V., Margolin, R., Monteith, J., Moser, C., Niu, Y.L., Pellé, H., Plank, T., Reynolds, J., Stuart, D., Thatcher, M., Wilson, C., Needham, H.D., Detrick, R., 1992. Rock and water sampling of the Mid-Atlantic Ridge from 32–41 °N: objectives and a new vent site. Eos 73 (43), 207.
Lowell, R.P., Rona, P.A., 2002. Seafloor hydrothermal systems driven by the serpentinization of peridotite. Geophys. Res. Lett. 29 (11), 1–4.
Marchig, V., Von Stackelberg, U., Wiedicke, M., Durm, G., Milovanovic, D., 1999. Hydrothermal activity associated with off-axis volcanism in the Peru Basin. Mar. Geol. 159, 179–203.
Michard, A., 1989. Rare earth element systematic in hydrothermal fluids. Geochim. Cosmochim. Acta 53, 745–750.
Mills, R.A., Elderfield, H., 1993. A dual origin for the hydrothermal component in a metalliferous sediment core from the Mid-Atlantic Ridge. J. Geophys. Res. 98 (B6), 9671–9681.
Mills, R.A., Clayton, T., Alt, J.C., 1996. Low-temperature fluid flow through sulfidic sediments from TAG: modification of fluid chemistry and alteration of mineral deposits. Geophys. Res. Lett. 23 (23), 3495–3498.
Ostwald, J., 1988. Mineralogy of the Groote Eylandt manganese oxides: a review. Ore Geol. Rev. 4, 1–43.
Parson, L., Grácia, E., Coller, D., German, C., Needham, H.D., 2000. Second-order segmentation; the relationship between volcanism and tectonic at de MAR, 38°N–35°40′N. Earth Planet. Sci. Lett. 178, 231–251.
Roy, S., 1981. Manganese Deposits. Academic Press, London, p. 458.
Schroeder, T., John, B., Frost, B.R., 2002. Geologic implications of seawater circulation through peridotite exposed at slow-spreading mid-ocean ridges. Geology 30, 307–367.
Severmann, S., Mills, R.A., Palmer, M., Fallick, A.E., 2004. The origin of clay minerals in active and relict hydrothermal deposits. Geochim. Cosmochim. Acta 68 (1), 73–88.
Sverjensky, D.A., 1984. Europium redox equilibria in aqueous solution. Earth Planet. Sci. Lett. 67 (1), 70–78.
Taylor, S.R., McLennan, S.M., 1985. The Continental Crust: its Composition and Evolution: an Examination of the Geochemical Record Preserved in Sedimentary Rocks. Blackwell Science Inc., Oxford, p. 312.
Toth, J.R., 1980. Deposition of submarine crusts rich in manganese and iron. Geol. Soc. Am. Bull. 91 (Part I), 44–54.
Usui, A., Bau, M., Yamazaki, T., 1997. Manganese microchimneys buried in the Central Pacific pelagic sediments: evidence of intraplaca water circulation? Mar. Geol. 141, 269–285.
Wildeman, T.R., Haskin, L.A., 1965. Rare-earth elements in ocean sediments. J. Geophys. Res. 70 (12), 2905–2910.
Zierenberg, R.A., Shanks, W.C., Bischoff, J.L., 1984. Massive sulfide deposits at 21° East Pacific Rise: chemical composition, stable isotopes, and phase equilibria. Geol. Soc. Am. Bull. 95, 922–929.
Zierenberg, R.A., Fouquet, Y., Miller, D.J., Bahr, J.M., Baker, P.A., Bjerkgard, T., Brunner, C.A., Duckworth, R.C., Gable, R., Gieskes, J., Goodfellow, D., Gröschel-Becker, H.M., Guèrin, G., Ishibashi, J., Iturrino, G., James, R.H., Lackschewitz, K.S., Marquez, L.L., Nehlig, P., Peter, J.M., Rigsby, C.A., Schultheiss, P., Shanks, W.C. III, Simoneit, B.R.T., Summit, M., Teagle, D.A.H., Urbat, M., Zuffa, G.G., 1998. The deep structure of a sea-floor hydrothermal deposits. Nature 392 (2), 485–488.